AGU PUBLICATIONS

JGR

Journal of Geophysical Research: Space Physics

RESEARCH ARTICLE
10.1002/2014JA020759

Key Points:
- Different types of electric field disturbances on a given night
- These include substorm, prompt penetration, and DP2-type events
- Impact on equatorial vertical drift and 630.0 nm airglow intensity

Correspondence to:
D. Chakrabarty,
dipu@prl.res.in

Citation:
Chakrabarty, D., D. Rout, R. Sekar, R. Narayanan, G. D. Reeves, T. K. Pant, B. Veenadhari, and K. Shiokawa (2015), Three different types of electric field disturbances affecting equatorial ionosphere during a long-duration prompt penetration event, *J. Geophys. Res. Space Physics*, *120*, doi:10.1002/2014JA020759.

Received 22 OCT 2014
Accepted 6 MAY 2015
Accepted article online 11 MAY 2015

Three different types of electric field disturbances affecting equatorial ionosphere during a long-duration prompt penetration event

D. Chakrabarty[1], Diptiranjan Rout[1], R. Sekar[1], R. Narayanan[1], G. D. Reeves[2], Tarun K. Pant[3], B. Veenadhari[4], and K. Shiokawa[5]

[1]Physical Research Laboratory, Ahmedabad, India, [2]Los Alamos National Laboratory, Los Alamos, New Mexico, USA, [3]Space Physics Laboratory, VSSC, Trivandrum, India, [4]Indian Institute of Geomagnetism, Navi Mumbai, India, [5]STEL, Nagoya University, Nagoya, Japan

Abstract Coordinated digisonde and OI 630.0 nm airglow observations from Thumba (TVM), an Indian dip equatorial station, in conjunction with magnetic and geosynchronous particle flux measurements, reveal three different types of electric field disturbances in the equatorial ionosphere-thermosphere system (ITS) occurring in succession over a period of 6 h on a single night (22–23 January,2012; A_p = 24). These include (1) westward electric field perturbations owing to a pseudo-breakup and a substorm event, each lasting for about 30 min; (2) eastward electric field perturbations continuing for about an hour, owing to the southward excursion of *Z* component of interplanetary magnetic field (B_z); and (3) DP2-type fluctuating (period ~40 min) electric field perturbation sustaining for about 4 h. The pseudo-breakup and the fully grown substorm events are found to be longitudinally localized and different in terms of response in the westward auroral electrojet index (*AL*) as well as geosynchronous electron/proton injections. The polarity of the prompt penetration of interplanetary electric field that affects the equatorial ionosphere is observed to be eastward during 2100–2200 IST (Indian Standard Time) which is observationally sparse but consistent with modeling studies. Interestingly, on the same night, DP2-type electric field fluctuations with ~40 min periodicity and occasional eastward polarity (akin to daytime) are also found to affect the equatorial ITS for about 4 h (2200–0200 IST). The case study, thus, brings out different processes that constitute a long duration prompt penetration event which, otherwise, would have been categorized as a single event.

1. Introduction

The zonal component of equatorial *F* region electric field is generally westward (eastward) during nighttime (daytime). Under quiescent geomagnetic conditions, this scenario does not change except during the June solstice of the solar minimum years when the *F* region zonal electric field, in a statistically significant manner, turns to the eastward direction for sometime during midnight hours [*Chakrabarty et al.*, 2014]. Prompt electric field perturbations during geomagnetic storms and magnetospheric substorms can affect the zonal electric field over equatorial region, and hence, these disturbances can alter the equatorial ionospheric electrodynamics in a significant manner. The altered zonal electric field plays an important role [*Chakrabarty et al.*, 2006; *Sekar and Chakrabarty*, 2008] in the generation of plasma irregularities in the equatorial ionosphere during local nighttime which is commonly referred to as Equatorial Spread F (ESF) events. Although these storm time disturbances are global in nature, the impact of these disturbances can have longitudinal and seasonal dependencies [*Fejer et al.*, 2008]. On the other hand, substorms occur in the nightside magnetotail and are known to be longitudinally confined on many occasions [*Belehaki et al.*, 1998].

Since the work of *Nishida* [1968], it has been acknowledged that the DP2 fluctuations due to the perturbations in the interplanetary magnetic field (IMF) can appear coherently all over the globe during geomagnetic storms. DP2 fluctuations are different from the fluctuations due to polar substorms (DP1) in the sense that they do not originate from the auroral electrojet similar to DP1. Subsequently, a number of investigations [e.g., *Fejer et al.*, 2007, and references cited therein] have reported DP2-type penetration electric field fluctuations as well as substorm-induced electric field fluctuations [*Kikuchi et al.*, 2003] in the equatorial ionosphere. Further, transient electric field disturbances due to storm sudden commencements have also been observed [*Sastri*, 2002]. In addition to these prompt electric field disturbances, delayed electric field perturbations owing to the disturbance dynamo effect [*Blanc and Richmond*, 1980] can also modify the equatorial ionospheric dynamics

at the later phase of a geomagnetic storm. Therefore, depending on the phase of the storm and the substorm, the space-weather-related electrodynamical effects on the equatorial ionosphere can be entwined in a complex manner. Although, these effects have been studied in isolation, decoupling of these effects will lead to comprehensive understanding of the critical aspects of the magnetosphere-ionosphere coupling on a global scale.

In order to address the prompt electric field disturbances on the equatorial ionosphere during space weather events, it is ideal to have direct electric field/vertical plasma drift measurements [e.g., *Kelley et al.*, 2003] by incoherent scatter radar. In the absence of incoherent scatter radar over the Indian sector, the temporal variations in the height of the equatorial *F* region can be interpreted as representing vertical plasma drift and used as a proxy for the zonal electric field. However, the ionosonde-derived drifts during nighttime can be significantly modulated by recombination effects especially when the base of the *F* layer height is below 300 km [*Bittencourt and Abdu*, 1981]. In addition, routine ionosonde observations may suffer from low temporal resolution. On the contrary, magnetometer observations can provide high temporal resolution and are primarily useful to study ionospheric effects during daytime. Low-latitude ionospheric conductivity is not large enough to support substantial currents during nighttime, and therefore, significant variations in the horizontal magnetic field over low latitudes during nighttime are believed to be due to the magnetospheric current variations [e.g., *Chakrabarty et al.*, 2005]. Photometric measurements of thermospheric airglow emission like OI 630.0 nm airglow emission can provide high temporal resolution and is reliable during nighttime in moonless, cloudless conditions.

In recent times, based on narrow band 630.0 nm nightglow photometry, it was shown [*Chakrabarty et al.*, 2005] that the periodicities of ~0.5 h and ~1.0 h in the interplanetary electric field (IEF) promptly penetrated into the low-latitude ionosphere. Further, transient electric field perturbations associated with the onset of the expansion phase of a magnetospheric substorm, captured by 630.0 nm dayglow measurements from low latitude, was also reported [*Chakrabarty et al.*, 2010]. These events brought out the effects of fast fluctuations in IEF and the ephemeral (lasting ~0.5 h) effects of induction electric field associated with the substorm dipolarization on the equatorial *F* region plasma dynamics. Interestingly, more often than not, changes in the solar wind drivers like polarity reversals in the interplanetary magnetic field (IMF) [*Lyons*, 1996] and/or sharp changes in the solar wind ram pressure trigger the onset of the expansion phase of magnetospheric substorms [*Lyons et al.*, 2008]. As IMF B_z condition significantly controls convection in the nightside plasma sheet during storms and the cross-tail current in the plasma sheet is generally believed to get altered during substorms, interaction between storm and substorm processes can impose electric field disturbances on the equatorial ionosphere which can be entwined at times making it difficult to identify the root mechanism. This problem is particularly severe during long-duration prompt penetration events [*Huang et al.*, 2005] when the probability of substorm occurrence is also high.

The present investigation originated from the need to explain the OI 630.0 nm airglow intensity undulations recorded over an Indian dip equatorial station during a magnetically disturbed night. While doing so, this study aims to delineate various magnetosphere-ionosphere coupling processes that occurred during a long-duration penetration event which otherwise would have been clubbed into a generic prompt penetration event associated with IMF B_z. The role of these prompt penetration electric fields in the generation of *F* region plasma irregularities is also explored.

2. Measurements and Supporting Data Set

2.1. The 630.0 nm Airglow Photometry

A coordinated experimental campaign involving two portable 630.0 nm airglow photometers and a collocated digisonde (DPS-4D) was conducted from Thumba, Trivandrum (TVM: Geog. Lat. 8.7°N, Geog. Long. 77°E, dip angle 0.5°N) during 18–30 January 2012. One of the photometers was looking toward the zenith direction and the other was designed (through mirror arrangement) to look toward eastern sky at a zenith angle of 45°. These airglow photometers were designed and fabricated at the Physical Research Laboratory, Ahmedabad, India. The airglow photometers described above have three sections, viz., front-end optics, filter section, and detector. The photometers employ f/2 optics. Temperature-controlled interference filters are used in the collimated section of the optical ray path. Both the photometers have narrow spectral bandwidth of 0.3 nm (around 630.0 nm) and field of view of 3°. A Hammamatsu made (H7421-40) photomultiplier tube (PMT) is used as a detector in the photometer that looks at the zenith direction (hereafter, zenith photometer). For the eastward viewing photometer (hereafter, east photometer), a different PMT (H7421-50) was used as a detector

because an identical PMT was not available during this campaign. Intensity fluctuations (and not the absolute intensities) are addressed in this work. The temporal resolutions of airglow intensity and ionograms are 5 s and 7 min, respectively.

2.2. Other Data Sets

The solar wind parameters (like solar wind velocity, density, magnetic field, etc.) are taken from the NASA GSFC CDAWeb (http://cdaweb.gsfc.nasa.gov/istp_public/) wherein these parameters are adjusted for the propagation lag up to the nose of the terrestrial bow shock. Based on the methodology described in *Chakrabarty et al.* [2005], the additional time lags consisting of magnetosheath and Alfven transit times (2 min) are incorporated point by point. This makes the solar wind parameters suitable for comparison with the ionospheric measurements. The temporal resolution of the solar wind parameters is 1 min although small intervals with "bad" data points are encountered sporadically during the period of interest. These points are removed. The *SYM-H* (symmetric ring current), *ASY-H* (asymmetric ring current), and *AL* (westward auroral electrojet) although taken from CDAWeb, have primarily come from WDC-C2 (Kyoto). The temporal resolution of these parameters is 1 min.

The horizontal magnetic field (H) variations over a few stations in the Indian and Japanese stations are used in the present study. The Indian stations include Tirunelveli (TIR; 3.3°N, 77.8°E, dip angle 0.5°N), Alibag (ABG; 18.6°N, 72.9°E, dip angle 26.4°N), and Jaipur (JPR; 16.9°N, 75.8°E, dip angle 41.9°N) and the Japanese stations include Kagoshima (KAG; 31.5°N, 130.7°E, dip angle 45.4°N) and Kototabang (KTB; 0.2°S, 100.3°E, dip angle 28.7°S). The temporal resolution of the H data is 1 min.

The Synchronous Orbit Particle Analyzer detectors on board the Los Alamos National Laboratory (LANL) geosynchronous satellites measure the energetic particle counts/fluxes in the near-Earth equatorial region at a nominal radial distance of 6.6 R_E (R_E, Earth's radius). These satellites are positioned around the geographic equator with an approximately fixed geographical longitude. In the present investigation, energetic electron and proton counts/s data are used. It is to be noted that particle flux = Counts/s × FCF (where FCF is a constant flux conversion factor for a given energy channel; FCF = detector efficiency at energy E × Geometric factor). Therefore, it is clear that the output signal in the form of counts instead of flux does not change the argument. Electron counts in four energy channels (E1: 48.15–69.85 keV; E2: 68.5–102.5 keV; E3: 99.95–149.45 keV; E4: 145.6–220.6 keV) and proton counts in three energy channels (P2: 75–11 keV; P3: 113–170 keV; P4: 170–250 keV), as measured by the LANL-02A and LANL-04A satellites, are used in this work. During the events discussed here, both these satellites were on the nightside.

3. Results

Figure 1a depicts the nocturnal variation of the base height of the *F* layer ($h'F$, in km) over Thumba (TVM) during 1900–0300 IST on 22–23 January 2012 (A_p = 24), The average morphological variations in $h'F$ over TVM during December solstice in solar minimum and maximum are reproduced from *Chakrabarty et al.* [2014] in Figures 1b and 1c. Figure 1d facilitates comparison between the *F* region vertical plasma drift (derived from the $h'F$ variation and in blue) and OI 630.0 nm airglow intensity over zenith (in red) recorded at Thumba on the same night. The *X* axis is in Indian Standard Time (IST) which is 5.5 h ahead of Universal Time (UT). Figure 1a reveals that there are conspicuous dips at ~2000 and ~2100 IST and a peak at ~2130 IST reaching 300 km altitude. Thereafter, $h'F$ starts decreasing from ~2200 IST onward. This decrease is observed up to ~0200 IST after which $h'F$ starts increasing again. It can be noted that the $h'F$ variations observed on 22–23 January 2012, are substantially different from the average morphological variations described in Figures 1b and 1c. The monotonic rise in $h'F$ associated with the prereversal enhancement (PRE) of eastward zonal electric field at ~2015 IST, as evident in the average variations, seems to be absent on this night. Instead, fluctuations in $h'F$ are seen during 1930–2100 IST and even beyond. The rate of change in $h'F$ ($dh'F/dt$) is used to derive the apparent *F* region vertical plasma drift. The true electrodynamical drift is obtained by subtracting the chemical loss contribution (βL) where β and L are the recombination rate and the plasma scale length, respectively. This has been done following the methodology of *Subbarao and KrishnaMurthy* [1994] with the exception that the L values are evaluated from the measured electron density profiles on this night. The *F* region vertical plasma drifts, thus obtained, are overlaid on the OI 630.0 nm airglow intensity fluctuations (zenith) in Figure 1d. It can be noticed that the two peaks (interspersed by a trough) in the airglow intensity during 2000–2100 IST are concomitant with downward vertical drifts (westward electric fields). The airglow intensity variation over a low-latitude station at this hour is generally marked by monotonic decrease [e.g., *Sekar et al.*, 2004] in the

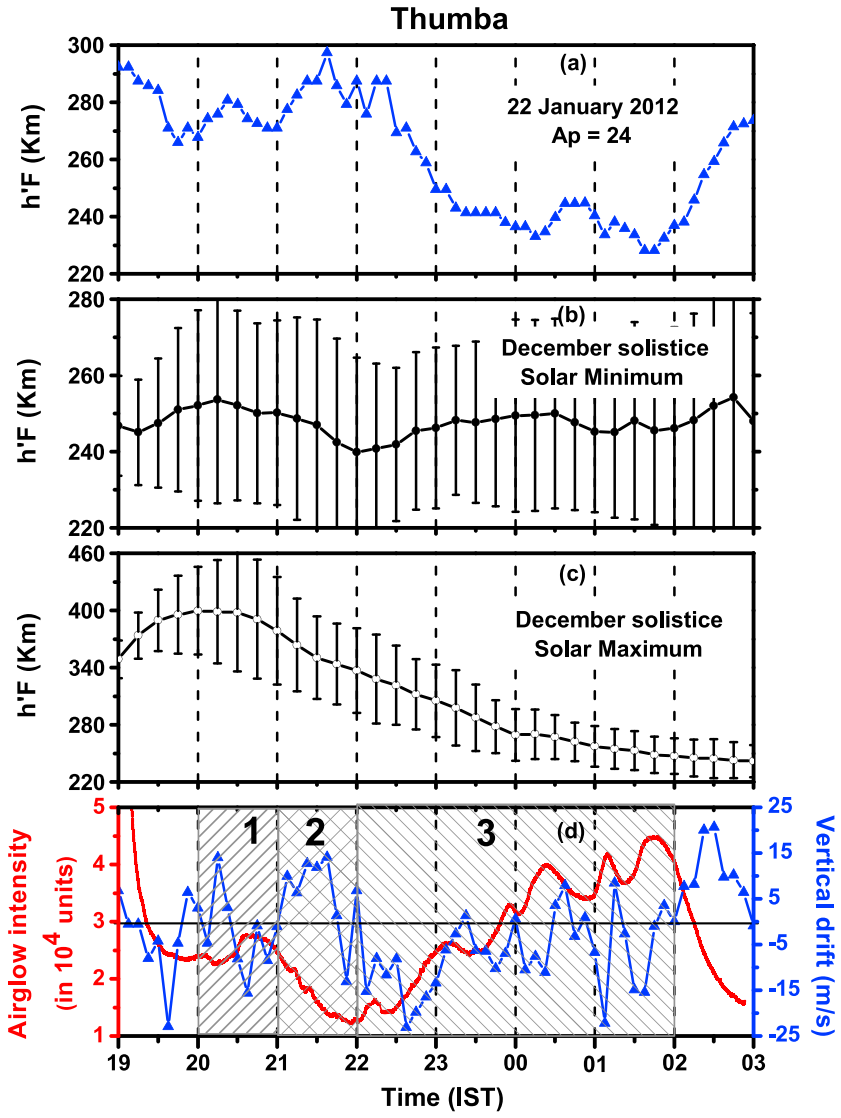

Figure 1. (a) Variation of $h'F$ (in km, in blue) during 1900–0300 IST (IST = UT + 5.5 h) on 22–23 January 2012 over Thumba, (b and c) morphological variations in $h'F$ over Thumba (taken from *Chakrabarty et al.* [2014]) along with the standard deviations during the December solstice in the solar minimum and maximum epochs, respectively, and (d) F region vertical plasma drift (recombination corrected, in blue) derived from the variations in $h'F$ on 22–23 January 2012 superimposed on the OI 630.0 nm airglow intensity variations (in red) recorded from Thumba. The three segments (1, 2, and 3), wherein the $h'F$ variations on this night are visibly different from the morphological variations, are marked by hatched lines (inclined to the right), cross-hatched lines and hatched lines (inclined to the left), respectively. The segments 1, 2, and 3 are characterized primarily by the westward electric field, eastward electric field, and DP2-type fluctuating electric field perturbations respectively.

absence of plasma irregularity events and geomagnetic disturbances. Clearly, the airglow intensity variations at 2000 and 2033 IST stand out as intensity enhancements. Interestingly, the monotonic decrease in the airglow intensity is observed during 2100-2200 IST which is associated with the upward drift (eastward electric field). Further, the undulations in the airglow intensity (six intensity peaks during 4 h) during 2200–0200 IST are just out of phase with the fluctuations in the vertical drift (fluctuations in the electric field). The drift fluctuations seem to precede the airglow fluctuations by 5 min. However, this time delay issue will not be addressed further as this is difficult to resolve, considering the temporal resolution of digisonde observation is 7 min. Based on the comparison of the F region vertical drift and 630.0 nm airglow intensity (Figure 1d), three distinctly different segments can be identified. Segment 1 (hatched lines inclined to the right) spans roughly between 2000 and 2100 IST when westward electric field perturbations are observed for at least 2 times corresponding to which airglow intensity shows enhancements. Segment 2 (cross-hatched lines) spans from

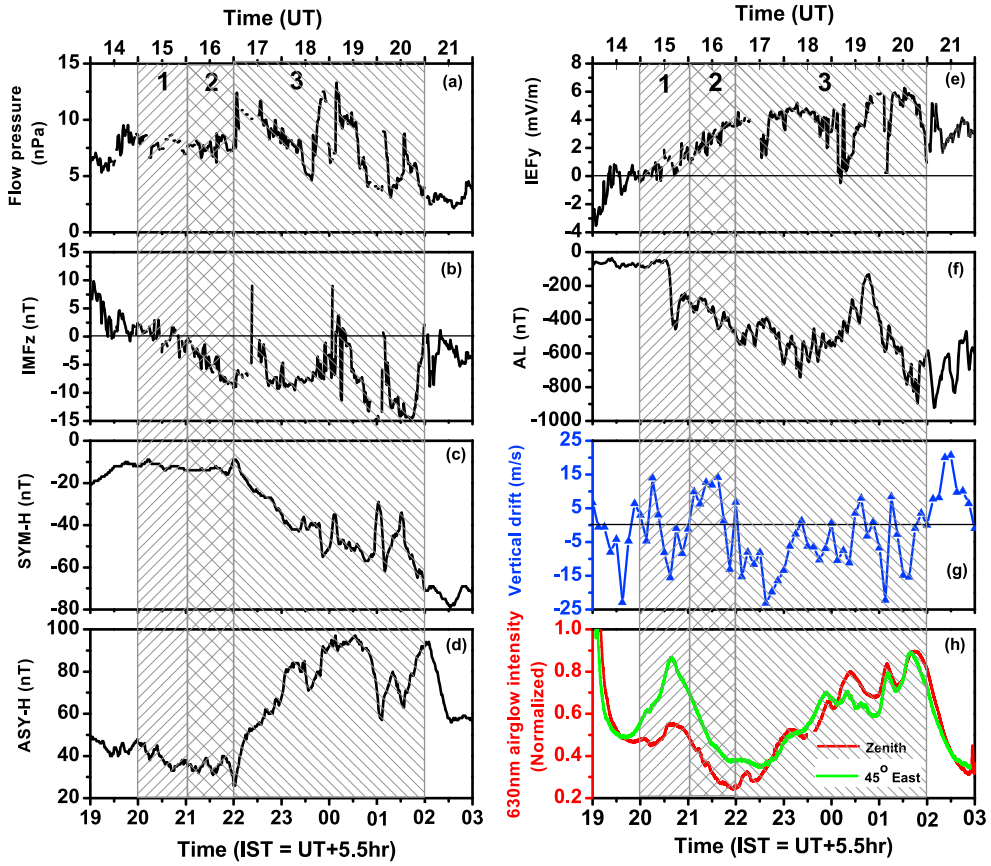

Figure 2. Variations in (a) solar wind flow pressure, (b) IMF B_z, (c) *SYM-H*, (d) *ASY-H*, (e) IEF_y (f) *AL*, (g) vertical drift (in blue), and (h) 630.0 nm airglow intensity from zenith (red) and 45° east (green) during 1900–0300 IST on 22–23 January 2012. Time in UT is also shown on top of the two panels. The three segments are also marked. One can notice the fluctuations in IMF B_z (and IEF_y) around the zero line in segment 1 before it fully turns to southward direction (IEF_y turns to dawn-to-dusk direction) in segment 2. Fluctuations in IMF B_z (and IEF_y) is noticed in segment 3. Intensification of *AL* starts at 2033 IST.

2100 to 2200 IST when eastward electric field perturbation is felt and airglow intensity reveals monotonic decrease. Segment 3 (hatched lines inclined to the left) is characterized by quasiperiodic fluctuations in drift and airglow intensity during 2200–0200 IST clearly under the influence of oscillating electric field.

Subsequent figures are presented to determine the cause of the fluctuations in the vertical drift and airglow intensity marked in segments 1–3 on 22–23 January 2012. Figures 2a–2h depict the temporal variation (in IST and corresponding UTs) of the solar wind flow pressure (in nPa), *Z* component (north-south) of the interplanetary magnetic field (IMF B_z) in nT, symmetric component of ring current as represented by *SYM-H* (in nT), asymmetric component of ring current as represented by *ASY-H* (in nT), *Y* component (dawn to dusk) of interplanetary electric field (IEF_y) in mV/m, westward auroral electrojet indices (*AL*), vertical drift (in m/s), and normalized 630.0 nm airglow intensity variations over zenith (red) and eastern (green, 45° zenith angle) directions. As the two photometers deploy detectors having different quantum efficiency and spectral sensitivity, the airglow intensity in each direction is normalized with respect to the maximum count in that direction for effective comparison of the temporal variabilities.

A number of interesting points can be noted based on Figure 2. The solar wind flow pressure does not change significantly during segments 1 and 2. *SYM-H* and *ASY-H* also do not change significantly during these intervals. At this juncture, it must be noted that the duration under consideration here falls under the main phase of a geomagnetic storm which starts at ~0800 UT on 22 January 2012 and ends at ~0500 UT on 23 January 2012. *SYM-H* values reach a minimum of ~ −90 nT at the end of the main phase after which a long recovery phase ensues. *AL* variation does indicate the onset of intensification (goes below −400 nT) of westward auroral electrojet at ~2033 IST (segment 1) on 22 January 2012. Two enhancements in airglow

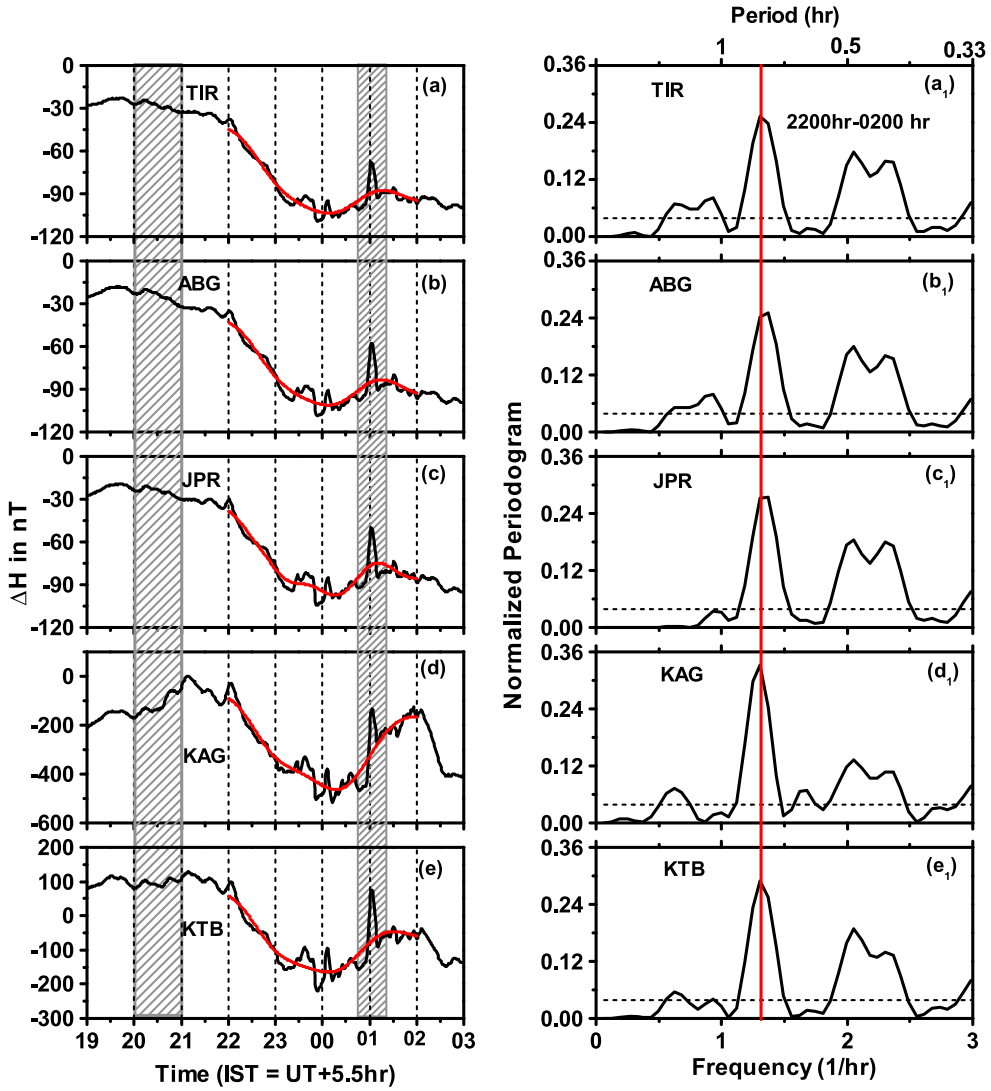

Figure 3. Variations in ΔH over the Indian and Japanese sectors during 1900–0300 IST on 22–23 January 2012. Indian stations are (a) Tirunelveli (TIR, dip angle 0.5°N), (b) Alibag (ABG, dip angle 26.4°N), (c) Jaipur (JPR, dip angle 41.9°N), and the Japanese stations include (d) Kagoshima (KAG, dip angle 45.4°N) and (e) Kototabang (KTB, dip angle 28.7°S). The two vertical-shaded boxes highlight the variations in ΔH during 2000–2100 IST (segment 1) and ~0100 IST. During segment 1, ΔH decreases over Indian stations and increases over Japanese stations. A sharp positive bay is seen at ~0100 IST over both Indian and Japanese stations. Note the identical fluctuations in ΔH during 2200–0200 IST (segment 3) over both Indian and Japanese stations. The smoothed variations during 2200–0200 IST are marked by red lines and overlaid on the actual variations. (a1–e1) The normalized periodograms of the fluctuations during the interval 2200–0200 IST. Periodicity of ~40 min is present over all stations.

intensity are observed at ~2000 IST and ~2033 IST during segment 1. These enhancements are associated with downward drifts, and the enhancement at ~2033 IST is also concomitant with intensification of *AL*. However, the airglow enhancement at ~2000 IST occurs when there are no substantial changes in the solar wind parameters and geomagnetic indices including *AL*. IMF B_z is found to be nominally northward at ~2000 IST and southward at ~2033 IST. During segment 2, IMF B_z does not show sharp fluctuations after turning southward. It is during this interval that vertical drift becomes predominantly upward in contrast to the downward drift expected [*Scherliess and Fejer*, 1999] during this time of the night. Airglow intensity variation over zenith reveals monotonic decrease during segment 2 which supports the upward drift during this interval. In segment 3, the quasiperiodic fluctuations are observed in the variations of IEF_y, vertical drift as well as in airglow intensity over zenith. The quasiperiodic fluctuations in airglow intensity cease to exist after 0200 IST. An interesting point must be noted here. The airglow intensity fluctuations in both the directions

during 2000–0200 IST are found to be nearly simultaneous. If one considers the centroid of airglow emission layer to be at 250 km, the zenith and 45° east in the sky are separated in the zonal direction by almost 250 km. Nevertheless, the undulations in the airglow intensity in both the directions have one-to-one correspondence without any appreciable time delay. On critical inspection, it can be noted that the relative amplitudes of the fluctuations differ in two directions particularly during 2000–2200 IST. The airglow enhancements at 2000 and 2300 IST are less conspicuous in the output of the photometer looking toward east as these enhancements are buried in larger emission volumes along the zonal slant path. The airglow variations in the east and zenith directions are also found to be slightly different during 0030–0100 IST. Despite these deviations, the overall similarities are striking and this additionally confirms that the intensity fluctuations addressed in the present case are related to the space-weather-related prompt electric field disturbances (and not to any zonal transport of plasma structures) that are expected to affect the two spatially separated regions in the sky nearly simultaneously.

Figure 3 depicts the variations in the horizontal component of magnetic field (ΔH) over the Indian and Japanese sectors during 1900–0300 IST. Two vertical-shaded boxes are overlaid on Figures 3a–3e to highlight the variations in ΔH during 2000–2100 IST and ~0100 IST. It is observed that ΔH decreases steadily over the Indian sector (particularly over JPR which is almost a midlatitude station) and increases steadily over Japanese sector (particularly over KAG which is a midlatitude station) during 2000–2100 IST. Smaller fluctuations in ΔH are also observed during this interval. These fluctuations are particularly prominent over Japanese sector and probably due to variations in the proton injection during 2000–2100 IST (see Figure 5). Interestingly, a pronounced positive bay is seen at 0100 h over all the stations in the Indian and Japanese sectors simultaneously. In addition to these variations, identical fluctuations in ΔH with no time delay are observed during 2200–0200 IST in all the stations that are widely separated in longitude as well as latitude. In order to find out the periodicity, the fast fluctuations in ΔH are extracted by using Savitzky-Golay (SG) smoothing algorithm [*Savitzky and Golay*, 1964]. The advantage of SG algorithm is its ability to enhance the signal-to-noise ratio without introducing significant distortion to the signal (in this case, the fast fluctuations). The smooth curves generated by the SG algorithm are marked by red line and overlaid on the ΔH variations during 2200–0200 IST. The fast fluctuations in ΔH, separated from the original variations, are subjected to harmonic analyses using a standard algorithm [*Schulz and Stattegger*, 1997]. The results of the harmonic analyses are shown in Figures 3a1–3e1. The "significant" spectral peaks stand over the "critical level" (marked by dashed horizontal line) determined by Siegel's test. Periodicity of 40 min (marked by vertical red line) is found to be "significant" and present over all the stations. Although other periods are also simultaneously present over all the stations, ~40 min periodicity is shown to be relevant for the equatorial ionosphere later.

The results of similar harmonic analyses of drift, airglow intensity fluctuations, and IEF_y data during segment 3 (2200–0200 IST) are depicted in Figures 4a–4c. It is found that ~40 min periodicity is present and "significant" in all the parameters. The black, blue, and red colors in Figures 4a–4c correspond to the spectra obtained from IEF_y, vertical drift, and 630.0 nm airglow intensity, respectively. Further, the results of detailed cross-spectral analyses between IEF_y and drift as well as IEF_y and airglow intensity are depicted in Figures 4d and 4e, respectively. These analyses generate the squared coherency and phase spectra for the two time series under consideration. Coherency is considered "significant" if it is close or more than the 95% false alarm level depicted by dashed line in the plots. "Significant" coherency with a stable phase relationship (around the periodicity to be tested) is considered necessary to infer causal relationship. It is found that the ~40 min periodicities in drift as well as in airglow are highly coherent with the ~40 min periodicity in IEF_y, and phase relationship is also nearly stable around this periodicity. This confirms that the 40 min periodicities in the equatorial drift and airglow intensity have its origin in IEF_y.

As stated earlier, two enhancements in airglow intensity are observed at 2000 IST and 2033 IST (segment 1). These enhancements in airglow intensity at ~2000 IST and 2033 IST are concomitant with downward drifts and hence with westward electric field disturbances. Interestingly, although the airglow intensity enhancement at 2033 IST is concomitant with the intensification of *AL*, a similar variation in *AL* is not seen during the airglow enhancement at 2000 IST. One reason could be that IMF B_z is northward at this time. In order to understand these aspects from a bigger perspective, the temporal variations (in UT as well as in IST which is UT + 5.5 h) in the electron counts/s at the geosynchronous altitudes by LANL-04A and LANL-02A satellites which were at ~70°E and ~103°E, respectively, at the nightside are presented in Figures 5a and 5b. So to say, LANL-02A was closer to midnight. Dispersionless injections of energetic electrons at geosynchronous orbit are observed by LANL-04A at 0100 IST. Similar injections are observed by LANL-02A satellite at 2000 IST and 0100 IST. Clearly,

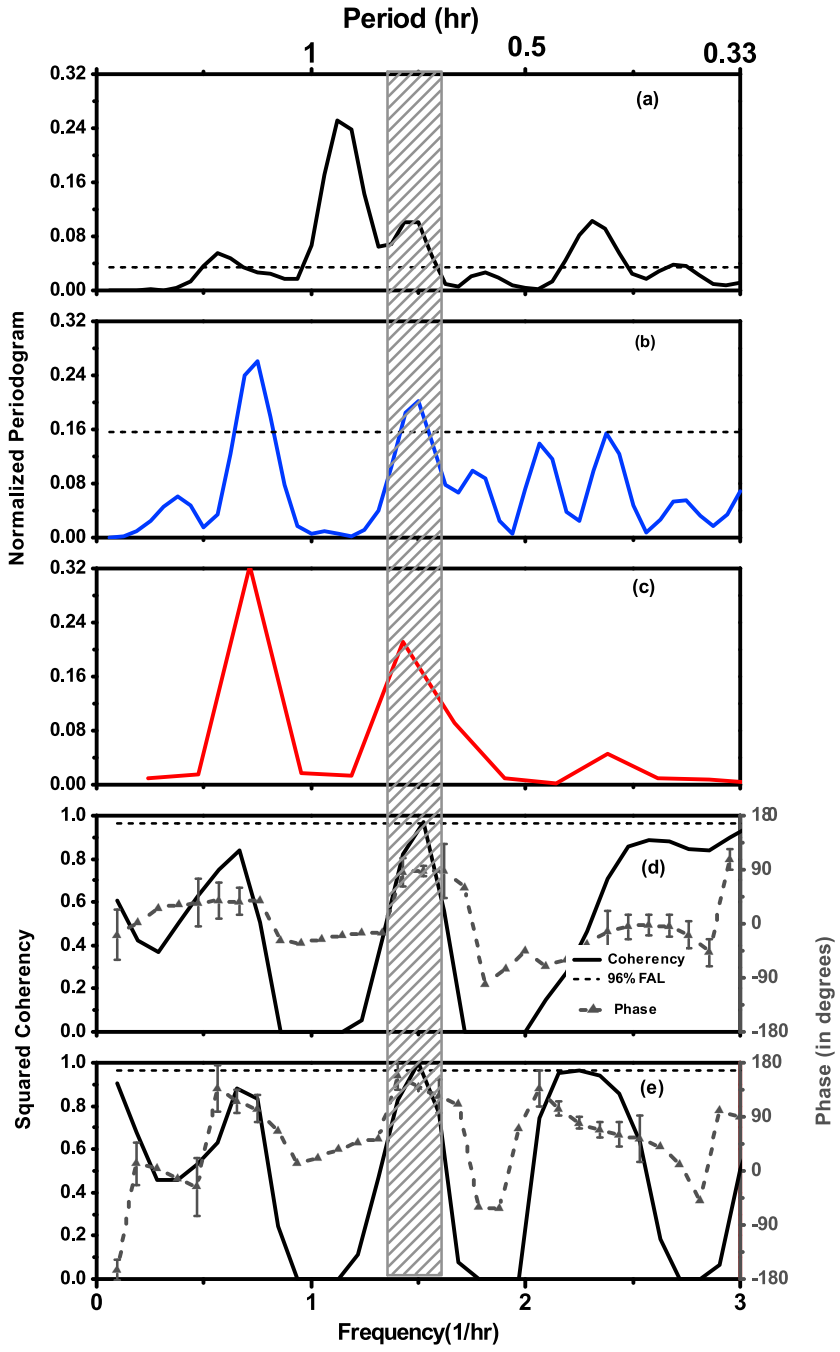

Figure 4. Normalized periodograms for the fast fluctuations in (a) IEF_y (in black), (b) vertical drift (in blue), and (c) 630.0 nm airglow intensity from zenith (in red) for the interval 2200–0200 IST (segment 3). Periodicity of 40 min is present in all the three parameters and is marked by the vertical-shaded box. Cross-spectral analyses between (d) IEF_y-drift and (e) IEF_y-airglow intensity reveal high (above the critical level marked by the dashed horizontal lines) coherencies and stable phase relationships between these pairs corresponding to 40 min periodicity. This suggests the role of IEF_y in causing the fluctuations in drift and airglow intensity.

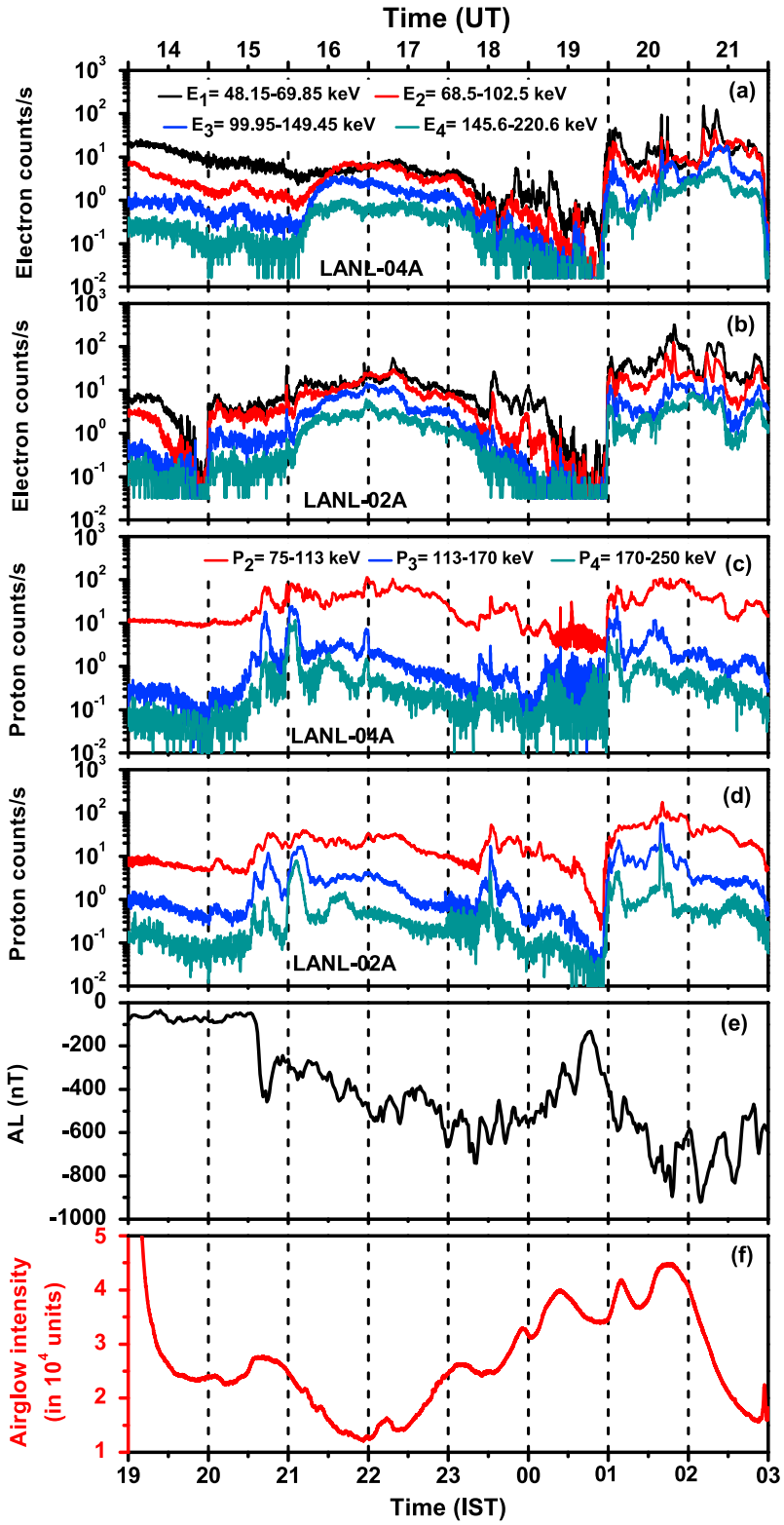

Figure 5. (a and b) Electron counts/s as measured onboard LANL-04A and LANL-02A, respectively. These satellites were on the Indian and Japanese sectors, respectively, during 1900–0200 IST. (c and d) Proton counts/s, as measured by these satellites. Dispersionless electron and proton injections are seen over Indian and Japanese sectors at 0100 IST. However, "dispersionless" electron injection at 2000 IST is seen only over Japanese sector. Proton injections are seen over both Indian and Japanese sectors at 2033 IST. Note that the onset of *AL* intensification is concomitant with this proton injection event.

the onset of the substorm at 2000 IST took place closer to the midnight sector and, hence, seen by LANL-02A but not picked up by LANL-04A. It is interesting to note that *AL* (Figure 5e) does not register any significant change at 2000 IST, although the airglow intensity over Indian dip equatorial region (Figure 5f) registers a small enhancement. Interestingly, when *AL* registers the onset of intensification at 2033 IST, there is no electron injection event observed by either LANL-04A or LANL-02A. However, downward plasma drift (Figure 2g) as well as enhancement in 630.0 nm airglow (Figure 2h) are observed over the dip equator at this time. In order to understand this aspect, proton injection events at the geosynchronous altitude, as measured by these satellites (Figures 5c and 5d), are investigated. It is found that onset of the substantial enhancement of proton injection starts at 2033 IST and detected by both LANL-04A and LANL-02A. Therefore, intensification of *AL* at 2033 IST seems to be concomitant with proton injection at the geosynchronous altitude and *AL* remains insensitive to "dispersionless" electron injection at 2000 IST detected by LANL-02A satellite. Interestingly, similar to the "dispersionless" electron injection event at 0100 IST, the proton injection event at 0100 IST is also found to be "dispersionless." *AL* starts weakening from 2330 IST when both the electron and proton counts start decreasing and eventually go to a negligible value before the onset of "dispersionless" injection at 0100 IST. Further intensification of *AL* starts after this injection event. In addition, it can also be noticed that although *SYM-H* and *ASY-H* respond to the "dispersionless" electron and proton injection events at 0100 IST, both these indices seem to remain unaffected by the "dispersionless" electron injection event at 2000 IST (Figures 2c and 2d, respectively). It is worth recalling at this juncture that ΔH decreases over the Indian sector and increases over Japanese sector during 2000–2100 IST and a pronounced positive bay is seen at 0100 h over all the stations in the Indian and Japanese sectors simultaneously. The implications of these results will be discussed in the ensuing section.

4. Discussion

The electric field disturbances during segment 1 brings out two enhancements (at 2000 IST and 2033 IST) in airglow intensity during 2000–2100 IST. This is clearly due to the downward plasma drifts over dip equatorial region as a consequence of the westward electric field disturbances associated with substorm activities during this interval. During this time, ΔH decreases over Indian longitudes and ΔH increases over Japanese longitudes. Further, LANL-02A satellite, which was longitudinally closer to Japanese longitude (~103°E), registers one "dispersionless" electron injection event at 2000 IST. However, there is no significant injection event at this time over Indian sector as suggested by the LANL-04A (~70°E) data. From these observations, it seems that the central meridian of the substorm current wedge (SCW) was over the Japanese sector during this event and Indian sector was outside the SCW. This explanation is offered for the following reasons.

The ground-based magnetic signatures associated with the onset of magnetospheric susbtorms are generally interpreted based on the substorm current wedge (SCW) model proposed by *McPherron* [1991]. Following this model, a positive bay in the ΔH-component variation is expected about the wedge central meridian and negative bay is expected outside the wedge. These predictions are consistent with observations also [*McPherron et al.*, 1973; *Sastri et al.*, 2003]. In the present investigation, ΔH decreases over the Indian sector and increases over the Japanese sector during 2000–2100 IST which provides a clue that the central meridian of the SCW might have been over Japanese sector (local midnight). Indian sector (local evening) could happen to lie just outside the formed SCW. This scenario is also consistent with the LANL observations as "dispersionless" injection is seen by the LANL-02A satellite at ~103°E but not seen by LANL-04A satellite at ~70°E.

Although these observations are consistent with the SCW model predictions, a few inconsistencies can also be noticed. If the event at 2000 IST is a substorm event, why there are no corresponding signatures in *SYM-H* and *ASY-H*? This casts doubt on the inference that the event at 2000 IST is a genuine substorm event or not. This doubt is further strengthened by the absence of corresponding enhancement of *AL* at this time. It is to be noted that LANL-02A observes "dispersionless" electron injection at this time. Therefore, this satellite seems to be inside the injection region. LANL-04A is further west at this time and the energy dispersion observed by this satellite indicates that this satellite was outside the injection region. It seems that there is a very narrow region where "dispersionless" events are seen for electrons but not for ions. Therefore, absence of enhancement in *AL* indicates the location of the injection region relative to the *AL* stations and also points toward the longitudinal confinement of this event. One of the possibilities could be that this event is a pseudo-breakup event and not a fully grown substorm event. Pseudo-breakups are known [*Pulkkinen et al.*, 1998; *Rostoker*, 1998] to be short-lived and localized substorm-like disturbances preceding the onset of the expansion phase of a full-fledged substorm. As the characteristic magnetospheric and ionospheric signatures corresponding to

the pseudo-breakups do not differ significantly from those of substorms, it is difficult to differentiate between these two processes [*Pulkkinen et al.*, 1998; *Rostoker*, 1998; *Sastri et al.*, 2003]. It is, however, argued [*Pulkkinen et al.*, 1998] that pseudo-breakups, more often than not, occur during the interval when the solar wind energy input into the magnetosphere is still going on. *Rostoker* [1998] argued that the pseudo-breakups have the normal characteristics of an expansive phase onset associated with a substorm but have amplitudes below some subjective limit. As a consequence, it is difficult to identify a pseudo-breakup event based on observations. *Rostoker* [1998], however, suggested that pseudo-breakups, phenomenologically, occur during a period of increasing energy input into the magnetosphere and "true" auroral break-ups occur during the release of stored tail energy that is accompanied with the decline in the rate of energy input into the magnetotail. Interestingly, in the present case, one can notice that although IMF B_z is generally northward around 2000 IST (even after considering maximum uncertainty of ~5 min in the propagation lag calculation), there were at least two very small southward excursions in the run-up to this event. This indicates interruptions in the energy input into the magnetosphere that might hinder the onset of a fully grown expansive phase. Therefore, the magnetospheric and ionospheric signatures at 2000 IST in the present case could very well be signatures of a pseudo-breakup event. Importantly, the westward electric field perturbations associated with this pseudo-breakup event gets registered in the 630.0 nm airglow intensity over dip equatorial station also. Further, "dispersionless" injections have also been observed in the past during pseudo-breakups [*Koskinen et al.*, 1993; *Nakamura et al.*, 1994; *Pulkkinen et al.*, 1998] similar to the present case.

The geosynchronous particle injection signatures at 2033 IST, when downward (westward electric field) *F* region plasma drift as well as airglow enhancement are observed over the Indian dip equatorial region, are also quite interesting. At this time, LANL-02A as well as LANL-04A satellite observations indicate absence of electron injections but presence of proton injections at the geosynchronous altitudes. It is at this time that *AL* shows sharp decrease below −400 nT (Figure 6). *Janzhura et al.* [2007] noted that in order to be classified as substorm, *AL* should exceed at least −400 nT during that event. This condition is satisfied in the present case. Further, *Reeves et al.* [1991] showed that "dispersionless" injections of protons may be observed independently on many occasions during substorms. This result is also supported by the test particle simulations of *Birn et al.* [1998]. *Chi et al.* [2006] also showed that proton auroral intensification at the onset of substorm and proton injection at the geosynchronous altitude can occur at the same magnetic local time (longitude). *Weygand et al.* [2008] demonstrated that the intensification of the westward auroral electrojet and the "dispersionless" particle injection can occur at about (within the uncertainty of the averages) the same time. Despite the geosynchronous injections and *AL* intensification, the substorm at 2033 IST in the present case does not seem to be associated with any sudden change in the solar wind parameters. It is found that even the maximum uncertainty of 5 min in the solar wind propagation delay does not change IMF B_z polarity at 2033 IST. Therefore, the substorm events do not seem to be associated with clear northward turning of IMF B_z. It is also verified that IMF B_y (not shown here) or solar wind dynamic pressure does not change significantly at and around this time. *Lyons* [1996] proposed that northward turnings of IMF B_z or reductions in IMF B_y or even enhancements in dynamic pressure [*Lyons et al.*, 2008] trigger most of the substorms. However, *Lee et al.* [2007] showed that some solar wind changes do not trigger substorms and it was suggested that the nontriggering types do not reduce the convection strength in the plasma sheet. In the present case, the role of IMF B_z (or other solar wind parameters) in triggering the substorm at 2033 IST is not clear and this requires further investigation. Nevertheless, the present observations strongly suggest the onset of the expansion phase of a substorm at ~2033 IST causing westward electric field disturbance as well as enhancement in 630.0 nm airglow intensity. It needs to be mentioned here that several authors [e.g., *Hashimoto et al.*, 2011, and references cited therein] invoked the important role of R2 FAC (region 2 field-aligned current) in determining the polarity of electric field disturbances on equatorial ionosphere at the substorm onset during both daytime and nighttime. The westward electric field disturbances on the nightside equatorial ionosphere at the substorm onset presented here is consistent with the narrative of *Huang et al.* [2004].

It is clear from Figure 1 that an upward drift (eastward electric field disturbance) is registered at ~2130 IST during segment 2 (2100–2200 IST) which is opposite in polarity (at this local time) if one compares it with the outputs of the Scherliess-Fejer model of quiet time equatorial *F* region vertical drift [*Scherliess and Fejer*, 1999]. In general, when the IMF is southward, IEF_y is positive (pointing dawn to dusk). Therefore, prompt penetration electric field is generally eastward on the dayside and westward on the nightside both pointing from dawn to dusk. Nevertheless, modeling calculations [e.g., *Nopper and Carovillano*, 1978; *Senior and Blanc*, 1984; *Tsunomura and Araki*, 1984] have indicated the presence of eastward penetration electric field as late as

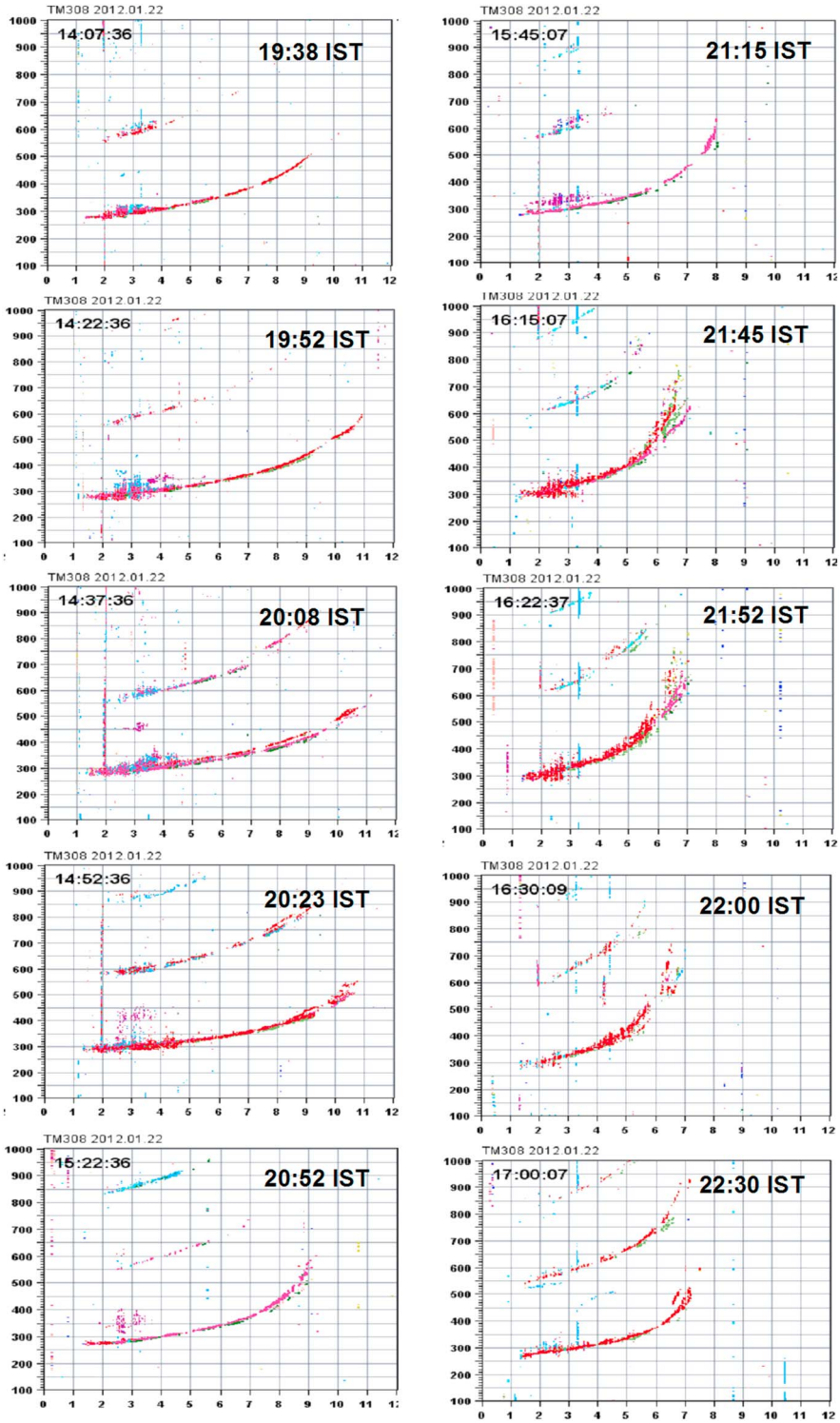

Figure 6. A series of ionograms obtained over Thumba during (left column) 1938–2052 IST and (right column) 2115–2230 IST. The left column shows the presence of weak range spread F at 1952 IST. The altitude extent of the spread decreases after the onset of the pseudo-breakup event at 2000 IST as seen from the ionogram at 2008 IST. The altitude extent of the spread increases after the pseudo-breakup event is over (see ionogram at 2023 IST). The altitude extent of the spread again decreases (see ionogram at 2052 IST) after the onset of the substorm at 2033 IST. The right column shows the presence of weak spread at 2115 IST which develops into an admixture of range and frequency spread F after the imposition of eastward prompt penetration electric field during segment 2 (2100–2200 IST). Interestingly, after the equatorial electric field becomes fully westward at 2230 IST, the spread F activity stops. No ESF activity is noticed during segment 3.

2200 LT. However, observational evidence in this regard is sparse. In addition, the polarity of overshielding electric field is generally westward during daytime and eastward during nighttime. As IMF B_z remains southward with increasing strength during 2100–2200 IST, the overshielding effect (associated with IMF B_z) is ruled out in the present case. Therefore, this is clearly a case of the effect of eastward prompt penetration electric field associated with IMF B_z turning steadily southward at this time. In this context, it is relevant to note that *Abdu et al.* [1998] and *Chakrabarty et al.* [2006] reported eastward prompt penetration electric field over Indian sector during dusk (1730–1900 LT) and 2030 IST, respectively. However, in the present case, this eastward prompt penetration electric field is felt as late as 2200 IST when quiet time ionospheric electric field polarity is expected to be westward. This is surely not a case of PRE getting enhanced as the electric field already turned to westward direction during post-sunset hours which can be seen from Figure 1d (~1930 IST). Therefore, the present case elicits that the polarity of the prompt penetration electric field can be eastward even during premidnight hours.

The consequences of the presence of westward and eastward electric field perturbations during segments 1 and 2 are also noticed from the critical inspection of the ionograms during these periods. Figure 6 is presented to highlight this aspect. The left column of Figure 6 shows a few representative ionograms during 1938–2052 IST. It can be noticed that a weak range spread F event was present at 1952 IST and which got subdued (reduction in the altitude extent of the spread) around 2008 IST indicating westward electric field influence due to the onset of the pseudo-breakup event at 2000 IST. The echoes developed with larger altitudinal extent at 2023 IST that indicated reduction in the westward electric field influence. The altitude extent of spread F echoes again got reduced at 2052 IST, owing to the influence of substorm-induced westward electric field perturbation. In order to highlight the eastward electric field perturbation during segment 2, the right column of Figure 6 is presented wherein a few representative ionograms during 2115–2230 IST are shown. It can be noticed that eastward prompt penetration electric field makes the range spread F event stronger and this is clear from the ionogram at 2115 IST. The weak range spread F event at 2115 IST then turns into an admixture of range and frequency spread F event (see the ionograms at 2145 and 2152 IST). Interestingly, once the influence of the eastward prompt penetration field ceases to exist after 2200 IST, the weak ESF event also comes to an end. This is amply evident from the ionogram at 2230 IST in which ESF is absent. Therefore, the westward and eastward electric field perturbations during segments 1 and 2 are also consistent with the evolution of weak ESF event on this night. It is to be noted here that ESF was absent during 2200–0200 IST and not responding to occasional eastward electric field probably due to lower *F* layer base height. It is known that the eastward electric fields assist the generalized Rayleigh-Taylor (GRT) instability which is known to be the prime causative mechanism of ESF. On the other hand, the westward electric fields inhibit the growth of GRT particularly at lower altitudes. The temporal pattern of the altitude extent of ESF echoes on ionograms in Figure 6 is consistent with the effects of electric fields on the development of ESF [e.g., *Sekar and Kelley*, 1998]. As the spread in the ionogram echoes during 1952–2200 IST start beyond 300 km altitude which is above the centroid of 630.0 nm emission, the airglow intensities are devoid of ESF signatures. This inference is strengthened by the absence of significant (a few tens of minutes) time delay between the points of mutual correspondence in the observed airglow intensities from zenith and eastern directions (see Figure 2h), indicating the origin to be due to space weather disturbances as mentioned earlier.

The last important aspect of this investigation is the prompt penetration of ~40 min periodicity in IEF_y into equatorial ionosphere (segment 3) that results in fluctuations in equatorial vertical drifts and corresponding 630.0 nm airglow intensity variations. As ~40 min periodicity is observed in the magnetic data simultaneously, the present observation probably provides a clear evidence of DP2 type fluctuations during midnight and postmidnight hours over equatorial region. The present case, similar to the case of *Sastri et al.* [2000] with the periodicity of 25–35 min, provides another evidence for DP2 type (occasionally eastward too) electric field perturbations affecting the dip equatorial ionosphere even during midnight hours. The eastward polarity (similar to daytime polarity) of the DP2 electric field during midnight hours is in contrast [e.g., *Sastri et al.*, 2000] to the expectation [*Tsunomura*, 1999] and requires further investigation. It is interesting to note that during the interval (segment 3) of DP2 type prompt penetration, a substorm onset also took place at 0100 h. This substorm onset conspicuously makes *SYM-H* less negative (see Figure 2c), causes enhancement in *ASY-H* (see Figure 2d), and generates clear positive bay in the ΔH variations over both Indian and Japanese sectors (see Figure 3). However, the influence of this substorm onset is difficult to delineate from the variations in the equatorial drift and 630.0 nm airglow intensity in the presence of the prompt penetration event. Therefore, it is not clear based on the present study how the substorm-induced electric field has modulated the prompt

penetration (of IEF_y) electric field during segment 3. This is a topic which requires further attention. In the context of prompt penetration of ~40 min fluctuation in IEF_y, the optical observation by *Sakai et al.* [2014] is pertinent. These authors recently presented 630.0 nm airglow intensity variations over Svalbard associated with polar cap patches during 1800–2400 UT on 22 January 2012. Although not reported by *Sakai et al.* [2014], ~40 min periodicity can be noticed in the observed 630.0 nm airglow intensity variation during 1800–2030 UT on this night. Therefore, it is clear that the ~40 min fluctuation in IEF_y has a global effect on this particular night and strengthens the argument for the DP2 origin of the fluctuations with similar periodicity observed over the equatorial region during midnight hours. Further, considering the theoretical shielding time constant to be ~20 min [*Senior and Blanc*, 1984], prompt penetration of 40 min fluctuations in IEF_y for 4 h into low-latitude ionosphere need further investigation on the magnetosphere-ionosphere coupling conditions that determine penetration events for longer duration.

5. Summary

Based on observations by multiple techniques, it is shown that three primarily different types of prompt penetration electric fields, occurring in sequence, have affected the equatorial ionosphere-thermosphere system over an interval of 6 h (2000–0200 IST) on a single night (22–23 January 2012). The salient points that have emerged from this investigation are as follows:

1. Westward electric field perturbations over Indian sector owing to a pseudo-breakup and a substorm event (each lasting for about 30 min) are identified. The substorm event follows the pseudo-breakup event. The effects of these magnetospheric events on equatorial *F* region zonal electric field are elicited and the evidences for the effects on nocturnal 630.0 nm airglow intensity over equatorial region are presented for the first time. Further, geosynchronous electron and proton signatures are also found to be different for these longitudinally confined magnetospheric events.
2. Observational evidence for eastward electric field perturbation (lasting for about an hour) as late as 2200 IST over Indian sector owing to the southward polarity reversal of IMF B_z, is presented. The upward *F* region vertical plasma drift (instead of the usual downward drift encountered during premidnight hours) and decrease in the 630.0 nm airglow intensity are consistent with eastward polarity of the penetration electric field. The eastward polarity of the electric field perturbation during premidnight hours is consistent with a few model predictions [e.g., *Nopper and Carovillano*, 1978; *Senior and Blanc*, 1984; *Tsunomura and Araki*, 1984] but observations are sparse in this regard.
3. Quasiperiodic (period ~40 min) fluctuations in the vertical drift and 630.0 nm airglow intensity over Indian sector (sustaining for about 4 h) are shown to have causal connection with the similar fluctuations in IEF_y. This is a possible signature of DP2 type electric field perturbations affecting the dip equatorial ionosphere even during midnight hours. Further, the occasional eastward polarity (similar to daytime polarity) of the DP2 electric field during midnight hours is in contrast with what is expected of equatorial DP2.
4. The investigation also captures the suppression of weak spread F under the effects of westward electric fields due to the pseudo-breakup/substorm events as well as the evolution of the range spread F event into an admixture of range and frequency spread F event due to the eastward prompt penetration electric field. It is also observed that occasional eastward polarity reversals during a DP2 type event do not trigger any plasma irregularity event during midnight hours probably due to low *F* layer base height.

Acknowledgments

This work is supported by the Department of Space, Government of India. The digisonde data used in this work are provided by Space Physics Laboratory, Vikram Sarabhai Space Center, Trivandrum, India. The Indian and Japanese magnetic data used in this work are provided by Indian Institute of Geomagnetism, Navi Mumbai, India, and Solar Terrestrial Environment Laboratory, Nagoya University, Japan, respectively. The geosynchronous particle injection data are provided by Los Alamos National Laboratory, New Mexico, USA. The geomagnetic indices and solar wind data are downloaded from NASA GSFC CDAWeb (http://cdaweb.gsfc.nasa.gov/istp_public/). The 630.0 nm airglow intensity data can be made available upon request for further evaluation and research.

Michael Balikhin thanks Kumiko Hashimoto and another reviewer for their assistance in evaluating this paper.

References

Abdu, M. A., J. H. Sastri, H. Luhr, H. Tachihara, T. Kitamura, N. B. Trivedi, and J. H. A. Sobral (1998), DP2 electric field fluctuations in the dusk-time dip equatorial ionosphere, *Geophys. Res. Lett.*, *25*(9), 1511–1514, doi:10.1029/98GL01096.

Belehaki, A., I. Tsagouri, and H. Mavromichalaki (1998), Study of the longitudinal expansion velocity of the substorm current wedge, *Ann. Geophys.*, *16*(11), 1423–1433, doi:10.1007/s00585-998-1423-9.

Birn, J., M. F. Thomsen, J. E. Borovsky, G. D. Reeves, D. J. McComas, R. D. Belian, and M. Hesse (1998), Substorm electron injections: Geosynchronous observations and test particle simulations, *J. Geophys. Res.*, *103*(A5), 9235–9248, doi:10.1029/97JA02635.

Bittencourt, J. A., and M. A. Abdu (1981), A theoretical comparison between apparent and real vertical ionization drift velocities in the equatorial F region, *J. Geophys. Res.*, *86*(A4), 2451–2454, doi:10.1029/JA086iA04p02451.

Blanc, M., and A. Richmond (1980), The ionospheric disturbance dynamo, *J. Geophys. Res.*, *85*(A4), 1669–1686, doi:10.1029/JA085iA04p01669.

Chakrabarty, D., R. Sekar, R. Narayanan, C. V. Devasia, and B. M. Pathan (2005), Evidence for the interplanetary electric field effect on the OI 630.0 nm airglow over low latitude, *J. Geophys. Res.*, *110*, A11301, doi:10.1029/2005JA011221.

Chakrabarty, D., R. Sekar, R. Narayanan, A. K. Patra, and C. V. Devasia (2006), Effects of interplanetary electric field on the development of an equatorial spread F event, *J. Geophys. Res.*, *111*, A12316, doi:10.1029/2006JA011884.

Chakrabarty, D., R. Sekar, J. H. Sastri, B. M. Pathan, G. D. Reeves, K. Yumoto, and T. Kikuchi (2010), Evidence for OI 630.0 nm dayglow variations over low latitudes during onset of a substorm, *J. Geophys. Res.*, *115*, A10316, doi:10.1029/2010JA015643.

Chakrabarty, D., B. G. Fejer, S. Gurubaran, T. K. Pant, M. A. Abdu, and R. Sekar (2014), On the pre-midnight ascent of F-layer in the june solstice during the deep solar minimum in 2008 over the indian sector, *J. Atmos. Terr. Phys.*, *121*, 177–187, doi:10.1016/j.jastp.2014.01.002.

Chi, E. C., S. B. Mende, M.-C. Fok, and G. D. Reeves (2006), Proton auroral intensifications and injections at synchronous altitude, *Geophys. Res. Lett.*, *33*, L06104, doi:10.1029/2005GL024656.

Fejer, B. G., J. W. Jensen, T. Kikuchi, M. A. Abdu, and J. L. Chau (2007), Equatorial ionospheric electric fields during the November 2004 magnetic storm, *J. Geophys. Res.*, *112*, A10304, doi:10.1029/2007JA012376.

Fejer, B. G., J. W. Jensen, and S.-Y. Su (2008), Seasonal and longitudinal dependence of equatorial disturbance vertical plasma drifts, *Geophys. Res. Lett.*, *35*, L20106, doi:10.1029/2008GL035584.

Hashimoto, K. K., T. Kikuchi, S. Watari, and M. A. Abdu (2011), Polar-equatorial ionospheric currents driven by the region 2 field-aligned currents at the onset of substorms, *J. Geophys. Res.*, *116*, A09217, doi:10.1029/2011JA016442.

Huang, C.-S., J. C. Foster, L. P. Goncharenko, G. D. Reeves, J. L. Chau, K. Yumoto, and K. Kitamura (2004), Variations of low-latitude geomagnetic fields and Dst index caused by magnetospheric substorms, *J. Geophys. Res.*, *109*, A05219, doi:10.1029/2003JA010334.

Huang, C.-S., J. C. Foster, and M. C. Kelley (2005), Long-duration penetration of the interplanetary electric field to the low-latitude ionosphere during the main phase of magnetic storms, *J. Geophys. Res.*, *110*, A11309, doi:10.1029/2005JA011202.

Janzhura, A., O. Troshichev, and P. Stauning (2007), Unified PC indices: Relation to isolated magnetic substorms, *J. Geophys. Res.*, *112*, A09207, doi:10.1029/2006JA012132.

Kelley, M. C., J. J. Makela, J. L. Chau, and M. J. Nicolls (2003), Penetration of the solar wind electric field into the magnetosphere/ionosphere system, *Geophys. Res. Lett.*, *30*(4), 1158, doi:10.1029/2002GL016321.

Kikuchi, T., K. K. Hashimoto, T.-I. Kitamura, H. Tachihara, and B. G. Fejer (2003), Equatorial counterelectrojets during substorms, *J. Geophys. Res.*, *108*(A11), 1406, doi:10.1029/2003JA009915.

Koskinen, H. E. J., R. E. Lopez, R. J. Pellinen, T. I. Pulkkinen, D. N. Baker, and T. Bösinger (1993), Pseudobreakup and substorm growth phase in the ionosphere and magnetosphere, *J. Geophys. Res.*, *98*(A4), 5801–5813, doi:10.1029/92JA02482.

Lee, D.-Y., L. R. Lyons, J. M. Weygand, and C.-P. Wang (2007), Reasons why some solar wind changes do not trigger substorms, *J. Geophys. Res.*, *112*, A06240, doi:10.1029/2007JA012249.

Lyons, L. R. (1996), Substorms: Fundamental observational features, distinction from other disturbances, and external triggering, *J. Geophys. Res.*, *101*(A6), 13,011–13,025, doi:10.1029/95JA01987.

Lyons, L. R., D.-Y. Lee, S. Zou, C.-P. Wang, J. U. Kozyra, J. M. Weygand, and S. B. Mende (2008), Dynamic pressure enhancements as a cause of large-scale stormtime substorms, *J. Geophys Res.*, *113*, A08215, doi:10.1029/2007JA012926.

McPherron, R. (1991), Physical processes producing magnetospheric substorms and magnetic storms, in *Geomagnetism*, vol. 1, edited by J. Jacobs, pp. 593–739, Academic Press, New York.

McPherron, R. L., C. Russell, and M. Aubry (1973), Satellite studies of magnetospheric substorms on August 15, 1968: 9. Phenomenological model for substorms, *J. Geophys. Res.*, *78*(16), 3131–3149.

Nakamura, R., D. N. Baker, T. Yamamoto, R. D. Belian, E. A. Bering, J. R. Benbrook, and J. R. Theall (1994), Particle and field signatures during pseudobreakup and major expansion onset, *J. Geophys. Res.*, *99*(A1), 207–221, doi:10.1029/93JA02207.

Nishida, A. (1968), Coherence of geomagnetic DP 2 fluctuations with interplanetary magnetic variations, *J. Geophys. Res.*, *73*(17), 5549–5559.

Nopper, R. W., and R. L. Carovillano (1978), Polar-equatorial coupling during magnetically active periods, *Geophys. Res. Lett.*, *5*(8), 699–702, doi:10.1029/GL005i008p00699.

Pulkkinen, T. I., et al. (1998), Two substorm intensifications compared: Onset, expansion, and global consequences, *J. Geophys. Res.*, *103*(A1), 15–27, doi:10.1029/97JA01985.

Reeves, G. D., R. D. Belian, and T. A. Fritz (1991), Numerical tracing of energetic particle drifts in a model magnetosphere, *J. Geophys. Res.*, *96*(A8), 13,997–14,008, doi:10.1029/91JA01161.

Rostoker, G. (1998), On the place of the pseudo-breakup in a magnetospheric substorm, *Geophys. Res. Lett.*, *25*(2), 217–220, doi:10.1029/97GL03583.

Sakai, J., K. Hosokawa, S. Taguchi, and Y. Ogawa (2014), Storm time enhancements of 630.0 nm airglow associated with polar cap patches, *J. Geophys. Res. Space Physics*, *119*, 2214–2228, doi:10.1002/2013JA019197.

Sastri, J. H. (2002), Penetration electric fields at the nightside dip equator associated with the main impulse of the storm sudden commencement of 8 July 1991, *J. Geophys. Res.*, *107*(A12), 1448, doi:10.1029/2002JA009453.

Sastri, J. H., H. Luhr, H. Tachihara, T. I. Kitamura, and J. V. S. V. Rao (2000), Electric field fluctuations (25–35 min) in the midnight dip equatorial ionosphere, *Ann. Geophys.*, *18*(2), 252–256, doi:10.1007/s00585-000-0252-2.

Sastri, J. H., Y. Kamide, and K. Yumoto (2003), Signatures for magnetospheric substorms in the geomagnetic field of dayside equatorial region: Origin of the ionospheric component, *J. Geophys. Res.*, *108*(A10), 1375, doi:10.1029/2003JA009962.

Savitzky, A., and M. J. Golay (1964), Smoothing and differentiation of data by simplified least squares procedures, *Anal. Chem.*, *36*(8), 1627–1639, doi:10.1021/ac60214a047.

Scherliess, L., and B. G. Fejer (1999), Radar and satellite global equatorial F region vertical drift model, *J. Geophys. Res.*, *104*(A4), 6829–6842, doi:10.1029/1999JA900025.

Schulz, M., and K. Stattegger (1997), SPECTRUM: Spectral analysis of unevenly spaced paleoclimatic time series, *Comput. Geosci.*, *23*(9), 929–945, doi:10.1016/S0098-3004(97)00087-3.

Sekar, R., and D. Chakrabarty (2008), Role of overshielding electric field on the development of pre-midnight plume event: Simulation results, *J. Atmos. Terr. Phys.*, *70*(17), 2212–2221, doi:10.1016/j.jastp.2008.04.015.

Sekar, R., and M. C. Kelley (1998), On the combined effects of vertical shear and zonal electric field patterns on nonlinear equatorial spread F evolution, *J. Geophys. Res.*, *103*(A9), 20,735–20,747, doi:10.1029/98JA01561.

Sekar, R., D. Chakrabarty, R. Narayanan, S. Sripathi, A. K. Patra, and K. S. V. Subbarao (2004), Characterization of VHF radar observations associated with equatorial spread F by narrow-band optical measurements, *Ann. Geophys.*, *22*(9), 3129–3136, doi:10.5194/angeo-22-3129-2004.

Senior, C., and M. Blanc (1984), On the control of magnetospheric convection by the spatial distribution of ionospheric conductivities, *J. Geophys. Res.*, *89*(A1), 261–284, doi:10.1029/JA089iA01p00261.

Subbarao, K. S. V., and B. V. KrishnaMurthy (1994), Seasonal variations of equatorial spread-F, *Ann. Geophys.*, *12*(1), 33–39, doi:10.1007/s00585-994-0033-4.

Tsunomura, S., and T. Araki (1984), Numerical analysis of equatorial enhancement of geomagnetic sudden commencement, *Planet. Space Sci.*, *32*(5), 599–604, doi:10.1016/0032-0633(84)90109-0.

Tsunomura, S. (1999), Numerical analysis of global ionospheric current system including the effect of equatorial enhancement, *Ann. Geophys.*, *17*(5), 692–706, doi:10.1007/s00585-999-0692-2.

Weygand, J. M., R. McPherron, K. Kauristie, H. Frey, and T.-S. Hsu (2008), Relation of auroral substorm onset to local AL index and dispersionless particle injections, *J. Atmos. Terr. Phys.*, *70*(18), 2336–2345, doi:10.1016/j.jastp.2008.09.030.